International Journal of Mechanical, Industrial and Aerospace Sciences
ISSN: 2517-9950
Vol:5, No:1, 2011

A Thermal-Shock Fatigue Design of Automotive Heat Exchangers

A. Chidley, F. Roger, A. Traidia

***Abstract*—** A method is presented for using thermo-mechanical fatigue analysis as a tool in the design of automotive heat exchangers. Use of infra-red thermography to measure the real thermal history in the heat exchanger reduces the time necessary for calculating design parameters and improves prediction accuracy. Thermal shocks are the primary cause of heat exchanger damage. Thermo-mechanical simulation is based on the mean behavior of the aluminum tubes used in the heat exchanger. An energetic fatigue criterion is used to detect critical zones.

***Keywords*—**Heat exchanger, Fatigue, Thermal shocks.

I. Introduction

TODAY'S mechanical designers of heat exchangers are faced with employing ever thinner material, yet working conditions become increasingly severe. Whilst pressure pulsations at the inlet can be very damaging, thermal shocks can also damage the structure within less number of cycles.
Although the heat exchanger is a very complex design, it is found that the first crack always appears on a tube which is at the inlet of the heat exchanger, where the thermal gradients are the highest. And furthermore it is at the junction between the tube and the collector (fig. 1).

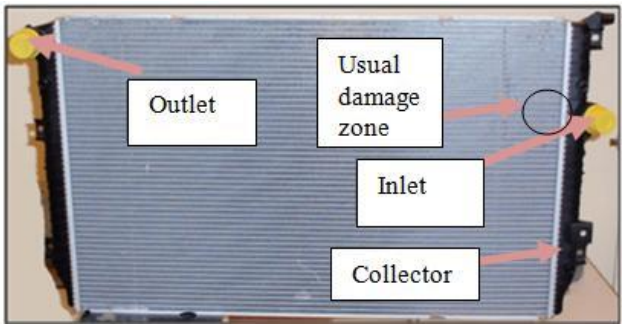

Fig. 1 Typical automotive heat exchanger

This paper describes how thermo-mechanical fatigue analysis can be used as a tool in the design of automotive heat exchangers (fig. 2). Actual thermal conditions are first defined, following which the mechanical behavior of the raw material is determined with a combined hardening behavior law, and finally a fatigue criterion is set to enable an estimation of product life. Thermo-mechanical simulation follows based on this empirical data. COMSOL Multiphysics finite elements software is used for all simulations.

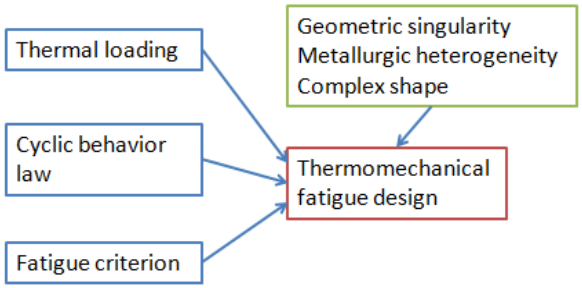

Fig. 2 Heat exchanger design method based on fatigue

II. Thermal Loading in a Heat Exchanger

To simulate real thermal conditions found in automobiles, a test bench system was set up where both the feed pressure and temperature are controlled. We filmed a stabilized thermal cycle using an InfraRed (IR) camera following work by [1]. Inlet conditions were set to known pressure and temperature values to be found within the heat exchanger during a typical trip.

Obtaining correct thermal imaging requires setting the emissivity of each material and its orientation. The emissivity was calibrated using a reference temperature probe.

Once the emissivity was set, we were able to read off the temperature with respect to time from any point on the film (Fig. 3).

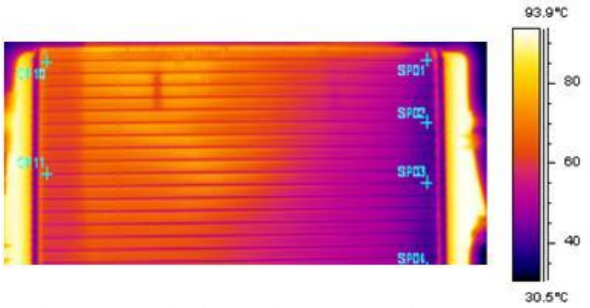

Fig. 3 Automotive heat exchanger as seen by an IR camera

A. Chidley is with Ecole Nationale Superieure de Techniques Avancees, F-91120 Palaiseau, France (e-mail: chidley@ ensta-paristech.fr).
F. Roger is with Ecole Nationale Superieure de Techniques Avancees, F-91120 Palaiseau, France (phone : 0169319815 e-mail: froger@ ensta-paristech.fr).
A. Traidia is with Ecole Nationale Superieure de Techniques Avancees, F-91120 Palaiseau, France (e-mail: traidia@ ensta-paristech.fr).

Figure 4 shows the thermal history at the inlet. This waveform is periodic and shows regions of constant temperature corresponding to stationary thermal loading.

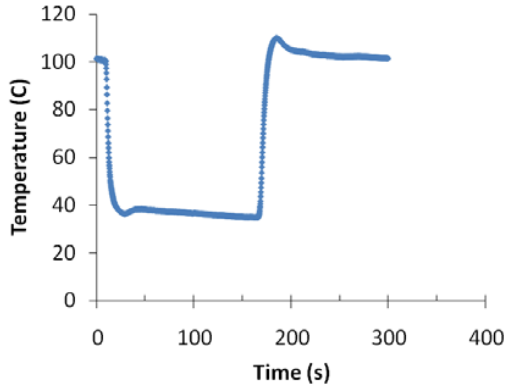

Fig. 4 Thermal history at the inlet over one stabilized cycle

As the maximum temperature is low (~100°C), we assume the mechanical behavior of aluminum alloys to be described by an elasto-plastic model neglecting any viscous phenomenon. In consequence, when the temperature is constant over time, the plasticity variables do not evolve; this allows considerable reduction in computing time by ignoring thermal history outside of the transient regions. Our experience is that damage is confined to a tube close to the inlet of the heat exchanger. As this damage occurs at the junction between tube and collector, we chose to focus on the extremity of the critical tube. Figure 5 depicts the computational domain within the tube and collector.

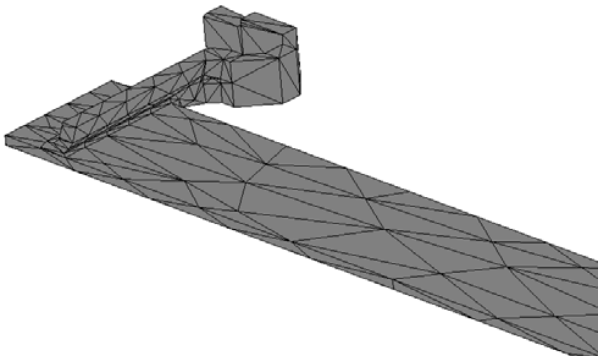

Fig. 5 Finite element model of a tube and part of the collector

The temperature gradients across the tube bundles within the heat exchanger is faithfully portrayed by IR imaging. Figure 6 shows the critical zone as seen by IR camera.

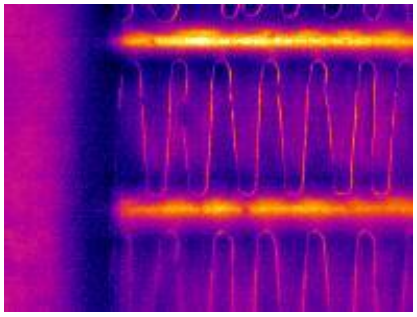

Fig. 6 Close up of the critical zone

Thermal shocks correspond to a sudden change in temperature. Using camera data we derive the following expression for temperature (T):

$$T(t,z) = 347.5 \pm \frac{75}{\pi}\tan^{-1}(200 * (\frac{z - 0.0125}{0.15} + \frac{t}{2})) \quad (1)$$

where the ± symbol corresponds to both hot and cold shock.

This function following perfectly both minimum and maximum values, slopes and cycle periods, is used for introducing source data into the mechanical simulation.

By employing a mathematical function to model thermal data, we avoid preliminary thermal calculation; in addition to obtaining a thermal field which better approaches reality, this greatly reduces calculation time.

III. Thermo Mechanical Modeling

The simulation technique employed translates thermal history into a thermal strain distribution. The elastic strain is computed using the following equation:

$$\varepsilon_e = \varepsilon - \varepsilon_{th} - \varepsilon_p \quad (2)$$

where ε_e is the elastic strain, ε the total strain, ε_{th} the contribution from the thermal field, and ε_p the plastic strain.

The Hookian relationship for stress evaluation can be written as follows:

$$\sigma = \left(K - \frac{2}{3}G\right)Tr(\varepsilon - \varepsilon_p - \varepsilon_{th})1 + 2G(\varepsilon - \varepsilon_p - \varepsilon_{th}) \quad (3)$$

Evaluation of the plastic strain requires complementary equations that describe the evolution of hardening variables [2].

$$\dot{\varepsilon}_p = \frac{3}{2}\dot{p}\frac{\sigma' - X'}{J_2(\sigma - X)} \quad (4)$$

$$f = J_2(\sigma - X) - R - \sigma_y \quad (5)$$

$$R = Q(1 - e^{-bp}) \quad (6)$$

$$\dot{X} = \frac{2}{3}C\dot{\varepsilon}_p - \gamma X\dot{p} \quad (7)$$

$$\dot{p} = \frac{1}{h}H(f)\langle\frac{3}{2}\frac{(\sigma' - X'):\dot{\sigma}}{J_2(\sigma - X)}\rangle \quad (8)$$

$$h = C - \frac{3}{2}\gamma\frac{(\sigma' - X'):X}{J_2(\sigma - X)} + b(Q - R) \quad (9)$$

K, G, σy, Q, b, C, and γ are constants depending only on the material used, described in table 1.

H(f) is the Heaviside function: H(f)=0 if f<0, and H(f)=1 if f≥0. ⟨a⟩ corresponds to the positive part of a.

X' and σ' are the deviators of respectively X and σ. And J2 is the second invariant of the stress deviator.

Substituting the calculated value of plastic strain into equation (2) provides us with a modified version of the classical elastic relationship in COMSOL.

Equation (4) describes the evolution of the plastic strain εp.

Equation (5) represents the yield surface.

Equation (6) calculates the isotropic hardening variable R.

Equation (7) is the PDE governing the kinematic hardening tensor X.

Equations (8) and (9) describe the evolution of the accumulated plastic strain variable p.

Due to normal manufacturing tolerances in the production of aluminium alloy heat exchangers, the behavior of different tubes is far from homogeneous. In consequence we have to define a mean material behavior in order to model the tube. Material characteristics are determined from tensile testing the raw tube material and substituted the values obtained into the elasto-plastic Chaboche [3] type law above.

The model used for simulation consists of one extremity of a thin tube; geometric and thermal symmetry allow us to simplify the model to a quarter of this tube. The boundary of our model comprises these axes of symmetry and a fixed border of the collector, the latter element providing rigidity within the heat exchanger assembly. The tube is not initially constrained, and the thermal field is set to the reference temperature.

IV. Fatigue Criterion

As the number of thermal shocks before fracture is low, the fatigue domain is considered to be olygocyclic. The criterion for olygocyclic fatigue can be based on either plastic strain ($\Delta\varepsilon_p$) or on dissipated energy during the life cycle [4]-[6].

We selected the latter due to its being both multi-axial and objective. This criterion allows calculation of the dissipated energy for each loading cycle, represented as a $\sigma(\varepsilon_p)$ function.

If this cycle reaches a stationary loop we can easily calculate the total amount of energy dissipated before fracture. This total dissipated energy corresponds to the number of cycles to fracture:

$$Wp = \int \sigma : \varepsilon_p dt \quad (10)$$

Once the stabilized cycle is obtained from cyclic modeling, our analytical approach enables the dissipated energy during each cycle to be determined, the critical element being identified by subsequent meshing. Moreover, if we identify the law between N (the maximum number of cycles) and Wp (energy) we can predict the life time of the structure.

V. Numerical Results and Discussion

A. Thermal field

Figure 7 shows the thermal field distribution during a hot shock.

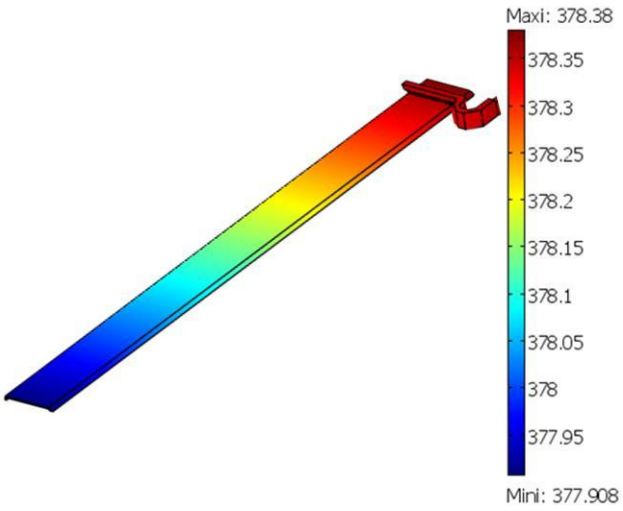

Fig. 7 Thermal gradient along the tube during a heating phase

B. Consequent mechanical conditions

The critical zones found using the Von Mises stress variable are confined to two main regions, both being situated at the joint between the tube and the collector, where the rupture always initiates. The reason is clear for the high stresses on the top surface, they correspond to the fixed conditions. Figure 8 depicts the localization of the maximum Von Mises stress.

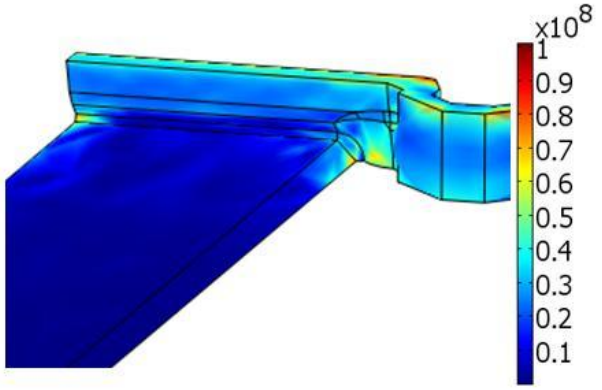

Fig. 8 Cartography of Von Mises stress after ten cycles

The cartography of cumulative plastic strain after ten cycles shows even more clearly that the maximum values appear within these critical zones. The cumulative plastic strain pinpoints the critical elementary volume in the mesh, as shown in figure 9.

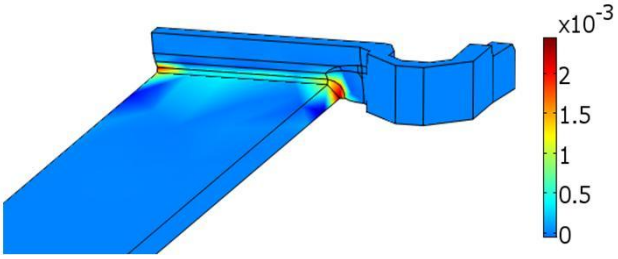

Fig. 9 Cartography of cumulative plastic strain after ten cycles

Once these zones are found, we can use the fatigue criterion to estimate the energy dissipated per cycle.

C. Cyclic behavior and fatigue design

Figure 10 shows the σ-ε cycles in the principal direction, at a point situated at the joint between the tube and the collector. The red line portrays the stabilized cycle, it shows that the structure does not remain elastic, and thus that we can use an energy fatigue criterion.

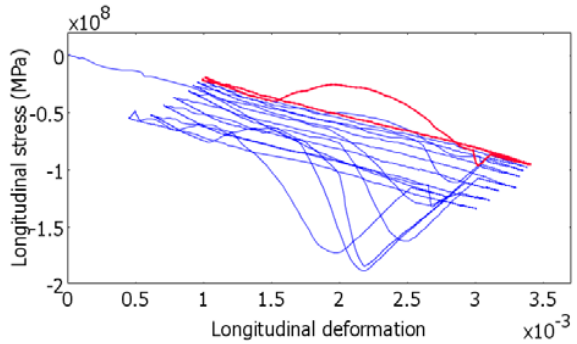

Fig. 10 σ-ε cycles in the principal direction, showing the stabilized cycle

Figure 11 represents the cumulative plastic strain at the critical point for each step in time. We can see that both the hot and cold shocks actively participate in moving the structure into the plastic zone.

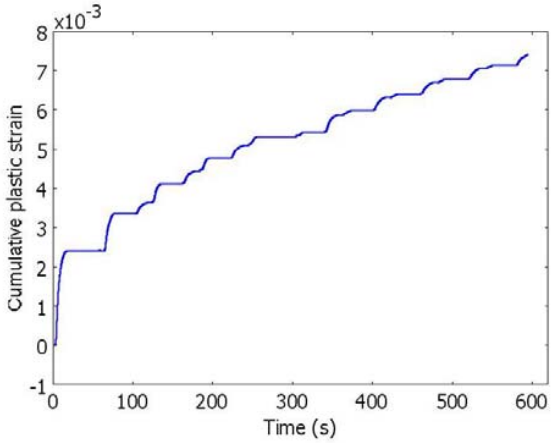

Fig. 11 Cumulative plastic strain in the critical zone for hot and cold shocks, showing the first 10 cycles

Figure 12 shows that a stabilized cycle is very quickly reached. It is not useful to carry on the simulation. Figure 12 represents the variation of σ:εp with time.

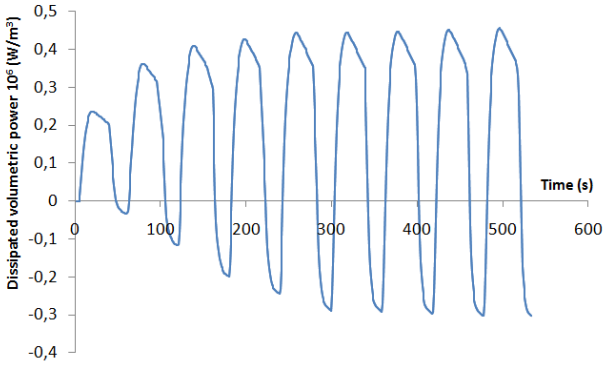

Fig. 12 volumetric power dissipated in the critical zone

The power is integrated over a cycle to obtain the volumetric energy. Figure 13 shows that the amount of energy dissipated at the critical zone can be measured precisely and used in fatigue design, provided that experimental tests are run using the same material, with simple geometric shaped test tubes.

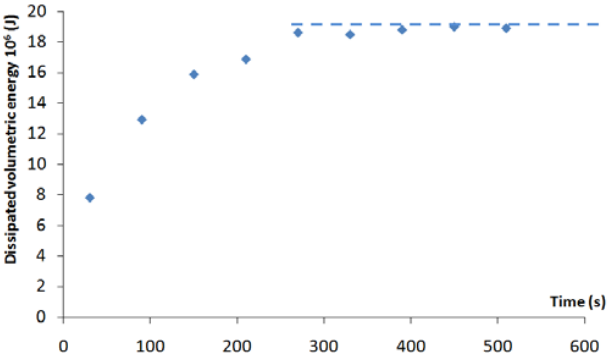

Fig. 13 Dissipated energy at each cycle

VI. Conclusion

The IR thermal imaging techniques employed in this study produced a precise thermal loading pattern and the calculation times are shorter than with preliminary coupled thermal fluid calculations.

The energy criterion chosen lets us consider the influence of all the stress tensor components, and also the whole history of the stress-strain distribution.

This is a more dynamic approach as opposed to a static analysis using a Von Mises criterion at a fixed time.

Acknowledgements

This research was supported by the French National Research Agency (ANR).

The authors are grateful to Valeo Engine Cooling for their help with the thermal shock experiments.

APPENDIX

TABLE I
ALUMINUM THERMAL AND ELASTO-PLASTIC PROPERTIES

Constant	Value	Unit
α	23e-6	1/K
E	69000	MPa
ν	0.33	
K	67500	MPa
G	20780	MPa
σy	70	MPa
Q	59	MPa
b	93.6	
C	11000	MPa
γ	600	

REFERENCES

[1] Herchang Ay, JiinYuh Jang, Jer-Nan Yeh, « Local heat transfer measurements of plate finned-tube heat exchangers by infrared thermography », International Journal of Heat and Mass Transfer, Volume 45, Issue 20, September 2002, Pages 4069-4078.
[2] Comportement élasto-plastique de Chaboche, Aster code.
[3] Lemaitre and Chaboche, Mécanique des Matériaux solides. Dunod (2009).
[4] Sébastien Amiable, Andreï Constantinescu, Stéphane Chapuliot & Antoine Fissolo, « Comparaison de modélisations numériques appliquées à une expérience de fatigue sous choc thermique », Colloque Giens 2005.
[5] A. Constantinescu, E. Charkaluk, G. Lederer, L Verger, « A computational approach to thermomechanical fatigue », International Journal of Fatigue 26 (2004), 805-818.
[6] **S.** Amiable, Stéphane Chapuliot, Andreï Constantinescu and Antoine Fissolo, « A comparison of lifetime prediction methods for a thermal fatigue experiment », International Journal of Fatigue Volume 28, Issue 7, July 2006, Pages 692-706.